Research article

Journal of RAMAN SPECTROSCOPY

Received: 21 November 2011 Revised: 10 January 2012 Accepted: 16 January 2012 Published online in Wiley Online Library: 4 July 2012

(wileyonlinelibrary.com) DOI 10.1002/jrs.4052

Degradation potential of airborne particulate matter at the Alhambra monument: a Raman spectroscopic and electron probe X-ray microanalysis study†

Sanja Potgieter-Vermaak,[a,b]* Benjamin Horemans,[c] Willemien Anaf,[c] Carolina Cardell[d] and René Van Grieken[c]

It is well known that airborne particulate matter (APM) has an impact on our cultural heritage. A limited number of articles have been published on the sequential application of elemental and molecular techniques to estimate the degradation potential of APM in environments of cultural heritage importance, and most of these were concerned with indoor environments. The Alhambra monument (Granada, Spain) represents one of the grandest and finest examples of Islamic art and architecture from the Middle Ages. As part of an air quality investigation, two sets of APM were collected at the Hall of the Ambassadors and characterised to determine its potential degradation profile. These were analysed by means of micro-Raman spectroscopy (MRS) and electron probe microanalysis with X-ray detection (EPXMA). The Raman data indicated the presence of various mixed salts of acidic and/or hygroscopic nature, such as sodium and ammonium nitrates and sulfates, especially in the finer fraction. Automated EPXMA estimated this fraction to be as high as 50%. Apart from the potential chemical attack, the soiling due to carbonaceous matter deposition is a real concern. Soot was identified by MRS and EPXMA in all size fractions, reaching values of up to 55%, and was often intertwined with soluble inorganic salts. Ongoing degradation of the pigments is implicated by the presence of brightly coloured particles. MRS and molar abundance ternary diagrams elicited the chemical structure of individual APM so that the degradation potential could be established. Copyright © 2012 John Wiley & Sons, Ltd.

Supporting information can be found in the online version of this article.

Keywords: airborne particulate matter; micro-Raman spectroscopy; EPXMA; degradation potential; monument

Introduction

The environmental impact of airborne particulate matter (APM) is determined not only by its mass and size distribution but also by its chemical composition. Furthermore, it is widely recognised that stressors, such as air pollution, form a direct link between the damage caused to our artistic heritage and the cultural environment.[1–4] It follows logically that effective preventive conservation can only be practised when all factors influencing the cultural environment are considered, including inherent synergisms. One of these factors with degradation potential that received some attention in previous papers is the chemical composition and structure of airborne particles.[3,5,6] The deposition of particles could cause changes to the surface, resulting, for instance, in surface discolouration due to soiling. Various publications report on carbonaceous-related soiling, e.g. level of soot particles necessary to observe soiling on coloured surfaces,[7] and black-crust formation on the surfaces of stone buildings.[2,8,9] In addition, chemical reactions at the particle/substrate interface can intensify the deterioration process as the particles act as condensation nuclei for gaseous pollutants as well as moisture. According to Brimblecombe,[1] this process can be described as a dose process that would encompass hydration, photodegradation, soiling, chemical attack, crystallisation stress, chemical transformation stress and dissolution. These processes affect the dyes (pigments) and surfaces of materials, resulting in fading or changing of colours, blackening, loss of contrast, rusting, weathering, etc. Clearly, the structural and chemical compositions of APM play an integral part in these dose processes and the resulting effects it has on the substrate.

A large number of articles are available on the chemical composition of APM,[10–16] but only a limited number of articles have been published on the sequential application of elemental and

* *Correspondence to: Sanja Potgieter-Vermaak, Division of Chemistry and Environmental Science, Manchester Metropolitan University, Chester Street, M1 5GD, Manchester, UK. E-mail: s.potgieter@mmu.ac.uk*

† *This article is part of the Journal of Raman Spectroscopy special issue entitled "Raman spectroscopy in art and archaeology" edited by Juan Manuel Madariaga and Danilo Bersani.*

a *Division of Chemistry and Environmental Science, Manchester Metropolitan University, Chester Street, M1 5GD, Manchester, UK*

b *Molecular Science Institute, School of Chemistry, University of the Witwatersrand, Private Bag X3, PO Wits, 2050 South Africa*

c *Department of Chemistry, University of Antwerp, Universiteitsplein 1, 2610, Antwerp, Belgium*

d *Department of Mineralogy and Petrology, University of Granada, Campus Fuentenueva s/n, 18071 Granada, Spain*

molecular techniques (such as the work by Potgieter-Vermaak *et al.*[17] and references therein), and those applied to APM in environments of cultural heritage importance are even fewer in number.[5,6,17] All of these deal with the influence of APM on indoor environments. Nava *et al.*[18] reported on the threat of air pollution at the Michelozzo Courtyard in Florence, but only mass and elemental concentrations and black carbon and water-soluble ion content are given. It is evident that both structural and chemical compositions of APM determine its degradation potential. Micro-Raman spectroscopy (MRS) is the ideal analytical technique to obtain such information on the molecular composition of APM as it provides the necessary fingerprint of the compound, which can then be correlated with spectral libraries as well as elemental information.[19] In addition, it is a nondestructive technique that provides the opportunity for further investigation of particles with, for example, ion chromatography, to obtain the water-soluble ionic composition.

As part of an air quality investigation, APM in the Alhambra was collected, and single particles were characterised to determine its potential degradation profile. The Alhambra represents one of the grandest and finest examples of Islamic art and architecture from the Middle Ages still standing in the developed world. The Alhambra was a fortified palatial citadel whose construction took place from the 11th to the 15th century, with the most outstanding palaces built during the Nasrid dynasty (1238–1492). Size-segregated APM was collected from a room in these palaces, and single-particle analyses were performed using MRS and electron probe X-ray microanalysis (EPXMA).

Experimental

Airborne environmental particles were collected inside the Hall of Ambassadors, one of the most outstanding rooms in the Nasrid palaces of the Alhambra monument (Fig. 1). This 'throne hall' was used by the sultans to welcome their eminent guests. It is a square hall with area of about 128 m^2 and height of 18 m. The walls of the hall have three arches, each leading to three small rooms with twin balconies and windows above. Polychromed stucco inscriptions of poems, mosaic tiling and a wooden ceiling describe the splendour of this hall. Although the 2.5-m-thick walls prevent the room from heating and keep it relatively cool during a hot summer day, the open entrance and windows (covered with wooden drawn works) do not protect the interior from ambient air.

One set of particles was collected on 7 July 2009 (summer) and another was collected on 9 February 2010 (winter), each representing the aerosol composition under typical meteorological conditions for the Granada region. Sampling was made by a seven-stage May-type cascade impactor to collect sets of size-segregated aerosols, optimising time of collection to ensure well-separated particles ready for single particle analysis. When operated at 20 l/min, the stages 1–7 have a 50% cut-off efficiency for particles with an equivalent aerodynamic diameter (d_a) of 0.25, 0.5, 1, 2, 4, 8 and 16 μm, respectively. Particles were collected directly on small pieces of silver foil. During summer, however, small particles (stages 1 and 2) were collected on silicon wafers. Two pieces of Ag/Si substrates were installed per stage in order to obtain parallel samples. Additionally, each stage was fitted with a small piece of a Nuclepore filter.

The low-Z elemental composition of the particles was analysed with electron-induced X-ray spectrometry, performed on an electron probe X-ray microanalyser (EPXMA, JEOL 733, Tokyo, Japan) coupled to an atmospheric ultra-thin window X-ray detector (Oxford, Abingdon, UK). The acceleration voltage, beam current and X-ray accumulation time were set at 10 kV, 1 nA and 10 s (automatic mode)/20 s (manual mode), respectively. In order to minimise the loss of volatiles, particles were cooled to liquid nitrogen temperature. Manual analysis of about 100 particles per sample (stages 1–2) and computer-controlled analysis of about 300 particles per sample (stages 3–6) resulted in 1388 and 1938 recorded X-ray spectra for particles collected in summer and winter, respectively. For each particle, the average diameter was calculated as $d_p = (d_{max} \times d_{min}^2)^{1/3}$, where d_{min} and d_{max} are the minimum and maximum Feret's diameters of the two-dimensional particle projections. Characteristic X-ray lines were used to classify particles into one of the four distinct aerosol classes listed in Table 1. It should be noted that the previously described approach is rather elaborate and intuitive as compared with commonly used multivariate classification methods.[20] However, although their strength lies in the mathematical algorithms on which they are based, the outputs of such

Figure 1. The Alhambra monument: (left) ground map of the monument and its surroundings and (right) view of the Hall of the Ambassadors (found inside the Comares tower) showing the stucco inscriptions with deteriorated polychromes.

Table 1. Particle classes and relevant compounds with their characteristic X-ray line profile

Class	Compound	Formula	Characteristic K_a, L_a lines (keV)
Minerals	Quartz	SiO_2	1.739(Si); 0.525(O)
	Feldspar	$XAlSi_3O_8$; X = Na, K	1.739(Si); 1.486(Al); 0.525(O); 1.041(Na); 3.312(K)
	Dolomite	$CaMg(CO_3)_2$	3.690(Ca); 1.253(Mg); 0.277(C); 0.525(O)
	Calcite	$CaCO_3$	3.690(Ca); 0.277(C); 0.525(O)
	Gypsum	$CaSO_4\ 2H_2O$	3.690(Ca); 2.307(S); 0.525(O)
	Iron oxide	FeO; Fe_2O_3	6.398, 0.705(Fe); 0.525(O)
Sea salts	Halite	NaCl	1.041(Na); 2.621(Cl)
	Sodium nitrate	$NaNO_3$	1.041(Na); 0.392(N); 0.525(O)
	Sodium sulfate	Na_2SO_4; $NaHSO_4$	1.041(Na); 2.307(S); 0.525(O)
SIA[a]	Ammonium nitrate	NH_4NO_3	0.392(N); 0.525(O)
	Ammonium sulfate[b]	$(NH_4)_2SO_4$; NH_4HSO_4	0.392(N); 2.307(S); 0.525(O)
	Ammonium chloride	NH_4Cl	0.392(N); 2.621(Cl)
Carbonaceous	Soot/organic	C, O-rich	0.277(C); 0.525(O)

[a]SIA, secondary inorganic aerosol. [b]Although indicated as a pure particle class, ammonium sulfate could not be distinguished from an ammonium sulfate/nitrate mixture solely on the base of characteristic X-ray lines.

techniques are often limited by the quality of the input variables. For example, depending on the loading of a sample, automated analysis often results in spectra of 'groups of particles'. Multivariate techniques would treat such a spectrum as equivalent to 'single-particle spectra' (disregarding the chemical relevance), which adds up to the total variance of the model. Such unsupervised problems are avoided in the direct classification of raw spectra, which only relies on the operators' knowledge of aerosol chemistry, and suffers less from losses in detail. With the spectra evaluated individually, about 80% were found to be useful for further processing, which corresponds to 1211 and 1521 particles in summer and winter, respectively. These spectra were evaluated by nonlinear least squares fitting with the AXIL code,[21,22] and the elemental composition (m/m%) of the particles was calculated with iterative simulations based on a reverse Monte Carlo procedure.[23,24]

MRS was performed on silver and Nuclepore substrates of stages 3, 5 and 6 in order to analyse the molecular composition of the particles, following best practices established as per Potgieter-Vermaak *et al.*[17,25] protocols. An InVIA spectrometer (Renishaw PTY Ltd.) utilising the 514.5-nm laser with maximum power of 50 mW (20 mW delivered at the sample) and a 100× objective (numerical aperture = 0.95; theoretical spot size of 0.36 μm) was used to ensure analysis of particles down to 0.5 μm. More than 50 individual particles were analysed per sample, to obtain representative results. Particles were located and analysed manually. Exposure time, number of acquisitions and laser power varied among 1–10 s, 1–100 and 2–10 mW, respectively. Data acquisition was carried out with the WireTM and Spectracalc software packages from Renishaw. Spectral searches were performed utilising an in-house, as well as commercially available, spectral libraries via Spectracalc software (GRAMS, Galactic Industries).

Results

Electron probe X-ray microanalysis

Particle size distributions of the summer and winter samples were quite similar (Fig. 2). From the linear tendency of the cumulative probabilities, it could be seen that the particle sizes are fairly well described by a lognormal distribution. Only probabilities for particles below 0.6 μm are lower than expected. This decreased probability for submicrometer particles is a consequence of the imaging resolution of the EPXMA ($d_p \geq 0.2$ μm), which results in data that are slightly left-censored. Nevertheless, both distributions could be used to evaluate the particle sizes at the Hall of the

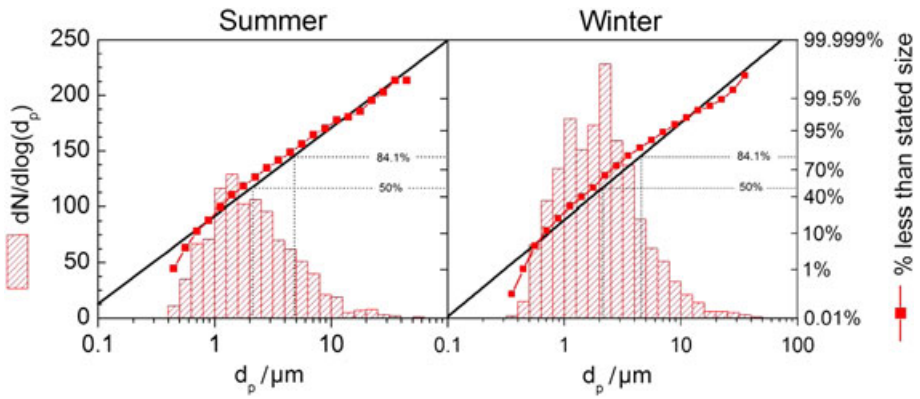

Figure 2. Particle number size distribution derived from the 2D particle projections in EPXMA. Geometric median: $d_p(50\%)$; geometric standard deviation (SD): $d_p(84.1\%)/d_p(50\%)$; geometric mean: median × exp(0.5 × $\ln^2$(SD)).

Ambassadors. Only one mode could be identified in both particle size distributions, which were characterised by a geometric mean standard deviation of 2.99 ± 2.5 and $2.7 \pm 2.2\,\mu m$ (median = 1.9 and 2.0 μm) for summer and winter, respectively. About 80% of the particles detected were larger than 1 μm. This distribution is similar to that observed by Shi *et al.*[26] during an Asian dust outbreak in Beijing, China (73% > 1 μm), and indicates how the smaller-diameter modes are overwhelmed by larger-sized mineral particles. Nevertheless, the bimodal nature of the APM at the Hall of the Ambassadors is clear from the number distribution and abundance plots for the four particle classes (Fig. 3). For particles with $d_a > 1\,\mu m$, mainly mineral and sea salt particles were found (70%–98%), whereas carbonaceous and secondary inorganic aerosols (SIA) represented the vast majority of particles with $d_a < 1$ μm (40%–76%). This strong difference between the chemical composition of submicrometer-sized and supermicrometer-sized particles was also found from the analysis of PM_1 and PM_{10} samples, as reported elsewhere[27] and agrees relatively well with the composition of APM found in other urban Mediterranean areas.[28]

Micro-Raman analysis

The MRS analysis revealed that particles with a d_a ranging from 4 to 8 μm (stage 5) were dominated by $NaNO_3$. This confirms the results of EPXMA analysis, where more than 55% of the particles in the considered size range were classified as sea salts during the winter campaign, in comparison with around 15% during summer (Fig. 3). $NaNO_3$ is produced in the atmosphere during atmospheric Cl replacement reactions on sea salt particles (NaCl).[29] In order to evaluate the extent of sea salt nitration and sulfation, the relative (molar) abundance of Cl, N and S (as obtained by EPXMA analysis) was plotted for each sea salt particle (Na-rich) as a ternary diagram (Fig. 4(a)). As could be seen, the majority of particles was rich in N ($NaNO_3$) and contained only traces of Cl (NaCl) and S (Na_2SO_4). Particles with more than 50% S (Na_2SO_4) were only found during winter, which is confirmed by its absence from the collected Raman spectra. Some of these sea salt particles proved to be laser sensitive[30] and were often intermixed with calcium sulfate present as gypsum, calcite and calcium nitrate (nitrocalcite), as illustrated in Fig. 5. This would suggest another class of particles, namely sea salts with calcium salts, which was not picked up from the EPXMA classification. Both campaigns' results for this size fraction also showed various dolomite-rich particles, often present with calcite and sodium nitrate, as illustrated in Fig. 6. This association of Ca and Mg was also illustrated by plotting a ternary diagram for the molar abundance of the Ca and Mg carbonate class (Fig. 4(b)). In addition, various sulfates associated with Ca were identified by MRS (illustrated in supporting information Fig. S1). The degree of sulfate formation on Ca and Mg carbonates can also be discerned from the ternary plot in Fig. 4(b). Two groups could be clearly distinguished: a S-poor group representing (almost) pure $CaCO_3$ and $MgCaCO_3$ particles and a group rich in S that clearly

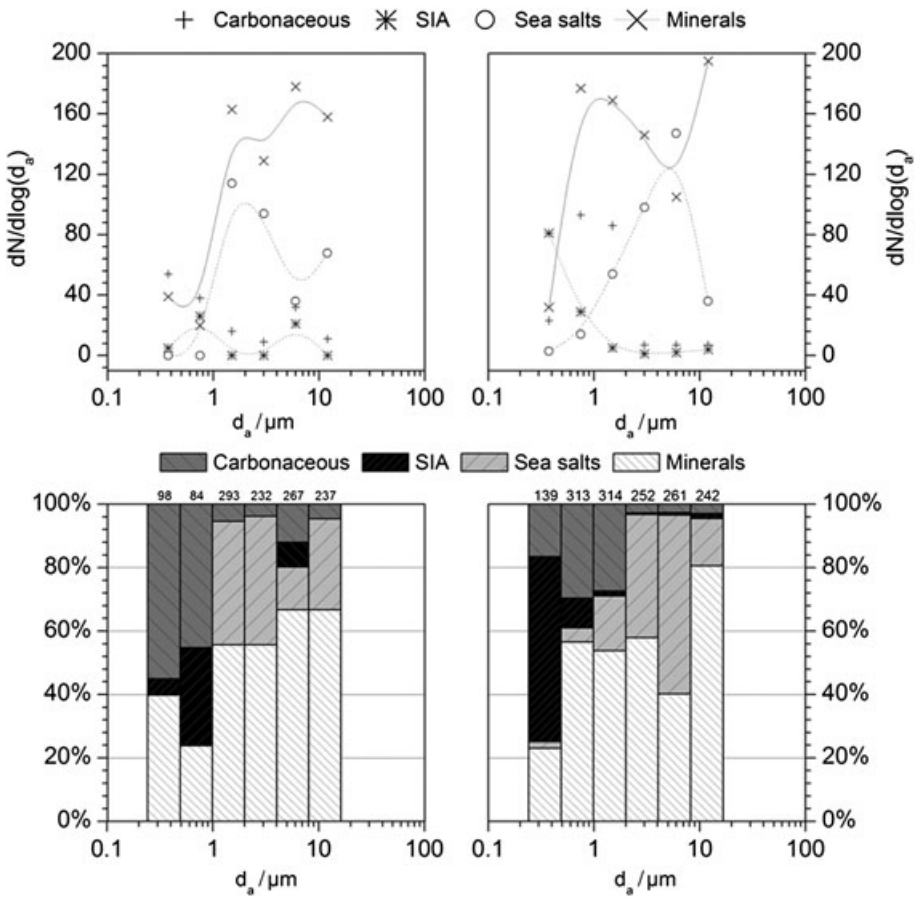

Figure 3. Particle number size distribution (top) and relative abundance plot (bottom) for the main classes of environmental aerosols during summer (left) and winter (right). Data were obtained with EPXMA. Aerodynamic diameter (d_a) size fractions between 0.25 and 16 μm correspond to the stages of the May impactor. For each size fraction in the abundance plot, the total number of analysed particles (*N*) is indicated on top of the corresponding column.

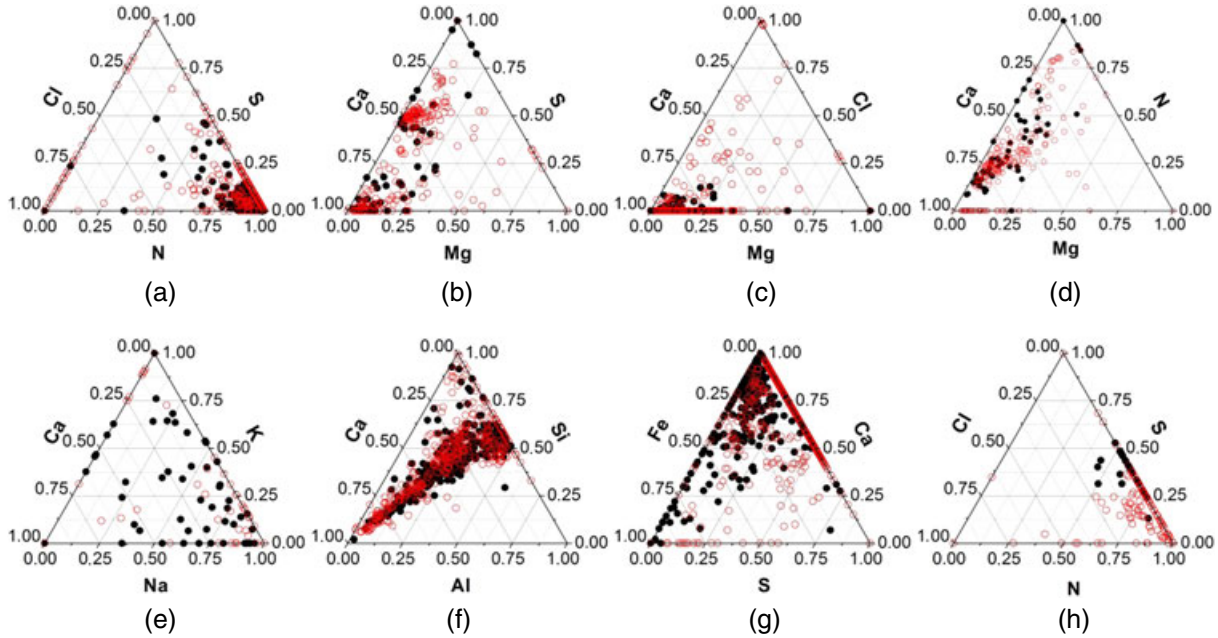

Figure 4. Ternary plots representing the relative (molar) abundance of some key elements measured by EPXMA in individual environmental particles: (a) sea salts (Na not shown), (b–d) Ca and Mg carbonates, (e) aluminium silicates, (f–g) mixed minerals and (h) secondary inorganic aerosols. Black closed markers: summer; red open markers: winter. This figure is available in colour online at wileyonlinelibrary.com/journal/jrs

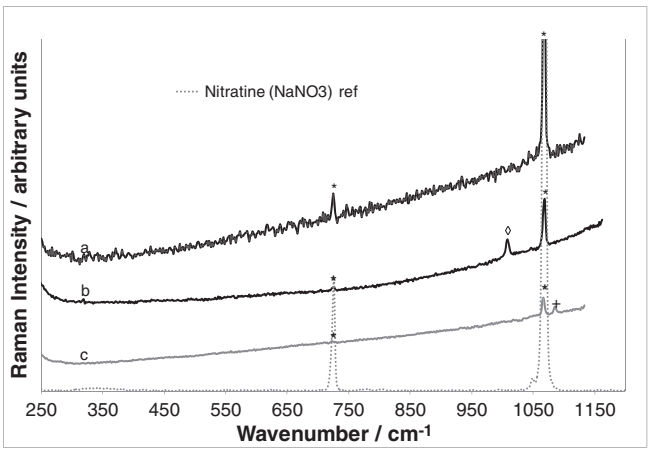

Figure 5. Raman spectra of sea salts and sea salt mixed with calcium salts ((a) nitratine (b) nitratine + gypsum; (c) calcite + nitratine) identified for particles with d_a ranging from 4 to 8 μm [* nitratine bands (1067 and 724 cm^{-1}); ◊ gypsum band (1008 cm^{-1}); + calcite band (1086 cm^{-1})].

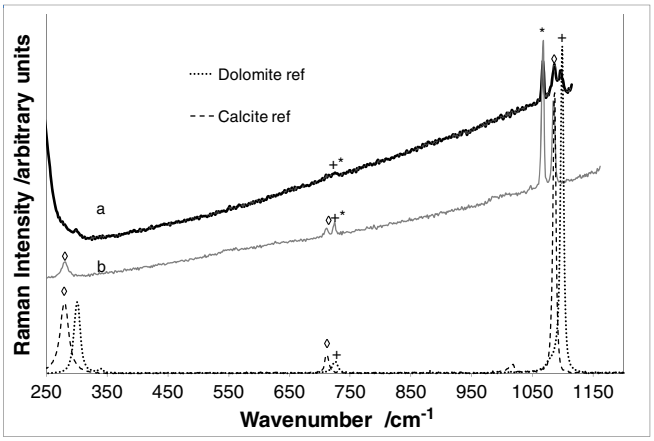

Figure 6. Raman spectra of various dolomitic particles ((a) calcite + nitratine + dolomite; (b) calcite + nitratine) from stage 5 (4–8 μm), displaying mixed salt character [*nitratine bands (1067 and 724 cm^{-1}); ◊ dolomite bands (1089, 724 and 399 cm^{-1}); + calcite bands (108, 712 and 280 cm^{-1})].

demonstrates the presence of some Ca and Mg sulfates (e.g. $CaSO_4$—anhydrite—or $CaSO_4.2H_2O$—gypsum). However, also $CaCl_2$ and $Ca(NO_3)_2$ were found to be present, as suggested by the Cl and N contents of these carbonates (Fig. 4(c,d)) and confirmed by MRS (Fig. 5). Various forms of iron oxides were also observed with MRS and identified according to the work of Colomban *et al.*[31] (spectra not shown). As can be expected, fair numbers of particles were identified as soot, especially from the winter campaign, by both optical microscopy and the characteristic G (graphitic) and D (disordered) Raman bands. The I_G/I_D ratios for these particles were on average 0.5, indicating a higher contribution of disordered carbon structure and less graphitic character. Soot particles were also often present with inorganic salts, such as gypsum, calcite, sodium nitrate and calcium nitrate, some of which are illustrated in Fig. 7. The EPXMA clusters only indicated pure carbonaceous clusters, and it was only with MRS that it could be discerned that inorganic salts were adsorbed onto the soot particles. As this fraction (stage 5; d_a from 4 to 8 μm) can be classified as medium fines, one would also expect presence of silicates, either as pure silica (quartz) or as aluminosilicates. From the elemental composition of the silicate class, about 18% of the particles were expected to be pure SiO_2 (quartz). The other silicates contained significant amounts of Al, i.e. about 90% was characterised by an Al-to-Si ratio ranging from 0.2 to 1. Because all contained some amount of Ca, Na and/or K (Fig. 4 (e)), the aluminosilicates were thought to be mainly feldspars. MRS indicated mostly the presence of α-quartz but always together with some aluminosilicates and never on its own.

The smaller particles investigated (stage 3; d_a from 1 to 2 μm) were dominated by sodium nitrate and soot in the summer, whereas the winter samples contained, in addition, gypsum,

Journal of RAMAN SPECTROSCOPY

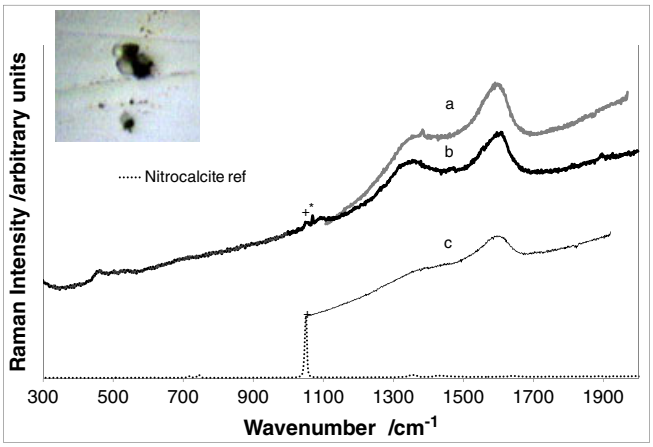

Figure 7. Raman spectra of amorphous carbon (probably soot) ((a) soot + ?; (b) soot + nitratine + nitrocalcite; (c) soot) identified on the stage 5 sample during summer [* nitratine band (1067 cm^{-1}); + nitrocalcite band (1050 cm^{-1})].

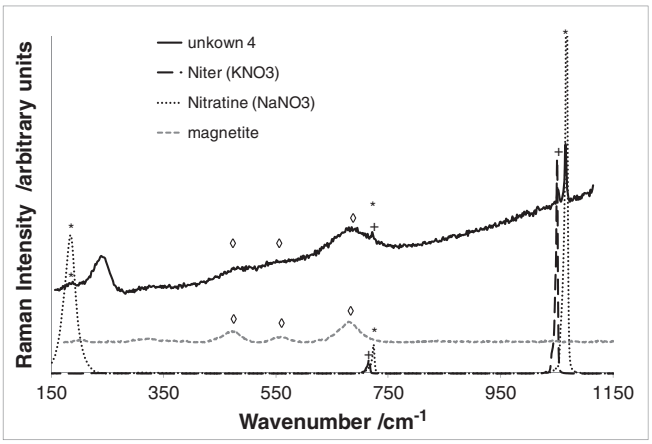

Figure 8. Raman spectrum of iron oxide (as magnetite, Fe_3O_4) mixed with KNO_3 and $NaNO_3$ at 1052 and 1066 cm^{-1}, respectively [* nitratine bands (1067 and 724 cm^{-1}); + niter bands (1050 and 716 cm^{-1}); ◊ magnetite bands (~470, ~566 and ~670 cm^{-1})].

calcium carbonate, iron oxides and carbonates in fair numbers. A number of brightly coloured particles where analysed, some of which showed not only different shades of blue but also various shades of orange, yellow and brown. The blue particles' spectra contained the symmetric stretch vibration of the S_3^- radical of lazurite/ultramarine blue at 545 cm^{-1}. These particles could be pigment particles that were detached from the walls. The yellow–orange–brown group of particles proved to be iron oxides together with sodium and potassium nitrates, as illustrated in Fig. 8. Again, a class of iron oxides mixed with sea salts were identified by MRS and not by EPXMA. The molar abundance ternary diagram for the mixed mineral particle class indicates that it was mainly composed of particles with a mixed content of both silicates and Ca/Mg carbonates (Fig. 4(f)). However, Fe oxides and sulfates were also found to contribute to their total mass (Fig. 4(g)).

For stage 2 (d_a from 0.5 to 1 μm), many ammonium sulfate particles, as well as various mixed ammonium salts (an example is given in supporting information Fig. S2), were identified. The identification of the double salt was based on values reported by Tang and Fung,[30] where it is reported that for the double salt, $(NH_4)_2SO_4NH_4NO_3$ will have main bands at 976 and 1043 cm^{-1} in contrast to the pure salts ($(NH_4)_2SO_4$ with main band at 976 and NH_4NO_3 with main band at 1050 cm^{-1}). The additional band at 1050 cm^{-1} could be either $Ca(NO_3)_2.4H_2O$ or pure NH_4NO_3 according to Tang and Fung.[30] The summer campaign's results showed only ammonium sulfate salts to be present, and no ammonium nitrate was identified nor any mixed ammonium salts in the 50 odd particles analysed. These results agree with the EPXMA single particle analysis results reported earlier. The molar abundance ternary diagram for the SIA particles, described by their Cl, N and S content (Fig. 4(h)), also suggests the same findings. During summer, Cl was generally absent in the particles. Because the share of N (relative to S) ranged from 50% to 75%, they were thought to be mixtures of NH_4HSO_4 and $(NH_4)_2SO_4$. The presence of NH_4HSO_4 was indicated in some instances by the presence of bands close to 960 and 1065 cm^{-1} as indicated by Tang and Fung,[30] but unambiguous identification could not be carried out. During winter, however, many particles were found with an N-share well above 75%, suggesting the presence of NH_4NO_3 (Cl = 0) and NH_4Cl (Cl > 0).

Discussion

MRS data elucidated and clarified the structural composition of many of the assumed elemental associations from the EPXMA data, using manual classification and molar abundance ternary diagrams. Examples are the dominance of $NaNO_3$ in the 4- to 8-μm fraction (stage 5), the presence of dolomitic particles and Ca–Mg carbonates in the presence of sulfates, and mixed ammonium salts in the fine fraction (stage 2; d_a from 0.5 to 1 μm). MRS also indicated that many of the particle types suggested by the EPXMA results were not pure and existed rather as mixed particles, for example, the iron oxides present with sea salts. These intertwined mineral and sea salt particles strongly suggest the presence of iberulites, i.e. microspherulites, which are exclusively found in the southern Iberian Peninsula.[32] These vortex-like particles (60–90 μm) consist of minerals and sea salts, formed during a Saharan dust outbreak. When collected on an impactor plate, iberulites splash into numerous smaller particles, which were recognised by MRS as mixed particles. In addition, the carbonaceous fraction (pure according to EPXMA) was shown to have various inorganic salts adsorbed onto it (illustrated in Fig. 7), which is of particular concern in terms of degradation potential.

In general, sea salts and alkaline Ca-rich minerals were found to be abundant in the Granada area. Under such conditions, any variation in the level of atmospheric acidifying gases should be buffered. One would expect that the use of heavy diesel fuel for domestic heating in Granada would result in elevated emissions of SO_2 and NO_2 during winter. Although no significant differences were observed in the level of these gases during both sampling campaigns,[27] the excess of atmospheric S and N was evident from the observed particle composition (Figs 4–8). The HCl, which is released during heterogeneous reactions between NaCl and SO_2/NO_2, is (partially) consumed by the excess of atmospheric $CaCO_3$ and NH_3, thereby recycling the escaped Cl^- to the solid phase, i.e. producing $CaCl_2$ and NH_4Cl.[33] Like NH_4NO_3, the latter is extremely volatile and will quickly evaporate at elevated temperatures. Therefore, NH_4NO_3 was not found with MRS, the EPXMA or molar abundance ternary plots during the hot summer (average indoor air temperature of 26 °C) but was only observed during the relatively cold winter (8 °C). The EPXMA results indicated the same tendency for NH_4Cl, but its presence or the lack of it was not confirmed by MRS. It is evident that the fine fraction contained large

concentrations of particles that are hygroscopic in nature (some of which also display acidic character) and therefore act as condensation nuclei.[34] This was especially true for the fine fraction, with the additional burden of high carbonaceous content, which have been shown to adsorb SIA particles easily. These particle sizes can also penetrate porous surfaces and lodge in crevices, which will exacerbate the damage that they could cause. An example is the discolouration of red lead (Pb_3O_4), a pigment found in the richly decorated Alhambra palaces.[35,36] In a humid atmosphere, the pigment has the tendency to form black plattnerite (PbO_2) and white cerussite ($PbCO_3$). However, the presence of salts such as $NaNO_3$, abundantly detected in the atmosphere surrounding the Alhambra site, promotes the conversion to these black-and-white reaction products.[37] Visually, this will lead to a more dull appearance of the initially bright red. Of course, the potential damage is proportional to the dose, which depends on concentration and exposure time. As the Alhambra monument and its splendour are constantly exposed to the elements and consequently APM, even at low ambient concentrations, one would expect high doses due to prolonged exposures. In addition, salt weathering of porous substrates (e.g. stucco and bricks) due to crystallisation–dissolution cycles may occur because of the presence of halite, sodium sulfate and nitratine.[38] It would therefore not be unreasonable to have concerns about soiling and chemical attack to the monument due to the large proportions of the fine APM that are carbonaceous and SIA rich to which the monument is constantly exposed.

Conclusions

Single particle analysis by EPXMA followed by either classification or clusterisation can only give elemental associations present in the particles and not the structural information required to discern their properties. MRS is an ideal analytical technique to further characterise heterogeneous individual particles, and one of the few techniques suitable for particles of submicron sizes. We have shown that the structural information obtained by MRS during this investigation confirmed some of the suggested elemental associations and elicited some new particle groups. Some examples of importance are the following: Na–N–O-rich clusters were indeed $NaNO_3$, N–O-rich clusters were NH_4NO_3, N–S–O-rich clusters were $(NH_4)_2SO_4$, Ca–C–O-rich were $CaCO_3$ and Mg–Ca–C–O-rich were dolomite. The elegant use of ternary diagrams, displaying the molar abundance of particle classes, added value to the results. Some of these salts (SIA and sea salts) are acidic and/or hygroscopic in nature, occur mainly in the finer fraction and could constitute up to 50% of the relevant fraction. The hygroscopic and/ or acidic nature of these particles will impact on various types of surfaces (causing weathering of stony materials, rusting of metal surfaces and discolouration of pigments due to chemical attack). Apart from the potential chemical attack, the soiling due to carbonaceous matter deposition is a real concern. Soot was identified by MRS and deduced from the EPXMA results in all size fractions (reaching values of up to 55% in the finest fraction during the summer campaign). MRS also showed that this particle class did not only contain amorphous carbons but that the soot was often intertwined with soluble and hygroscopic inorganic salts. This observation confirmed that soot acts as an adsorbent, providing a substrate for APM and, as such, exacerbates degradation potential. The identification of brightly coloured particles, such as lapis lazuli, could be evidence of ongoing degradation of the pigments present in the building.

Acknowledgements

The authors thank the research group RNM-179 (CICE, JA, Spain) and the 'Patronato de la Alhambra y Generalife' for making this research possible.

Supporting information

Supporting information can be found in the online version of this article.

References

[1] P. Brimblecombe, in Cultural Heritage Conservation and Environmental Impact Assessment by Non-Destructive Testing and Micro-Analysis, (Eds: R. Van Grieken, K. Janssens), Leiden, Balkema, **2005**, p. 11–18.
[2] A. Bonazza, C. Sabbioni, N. Ghedini, *Atmos. Environ.* **2005**, *21*, 2607–2618.
[3] V. Kontozova-Deutsch, C. Cardell, M. Urosevic, E. Ruiz-Agudo, F. Deutsch, R. Van Grieken, *Environ. Earth Sci.* **2011**, *63*, 1433–1445.
[4] I. Ozga, A. Bonazza, E. Bernardi, F. Tittarelli, O. Favoni, N. Ghedini, L. Morselli, C. Sabbioni, *Atmos. Environ.* **2011**, *45*, 4986–4995.
[5] A. Worobiec, E. A. Stefaniak, V. Kontozova, L. Samek, P. Karaszkiewicz, K. van Meel, R. Van Grieken, *e-Preserv. Sci.* **2006**, *3*, 63–68.
[6] R. H. M. Godoi, S. Potgieter-Vermaak, A. F. L. Godoi, M. Stranger, R. Van Grieken, *X-Ray Spectrom.* **2008**, *37*, 298–303.
[7] L. M. Bellan, L. G. Salmon, G. R. Cass, *Environ. Sci. Technol.* **2000**, *34*, 1946–1952.
[8] S. S. Potgieter-Vermaak, R. H. M. Godoi, R. van Grieken, J. H. Potgieter, M. Castillejo, *Spectrochim. Act A* **2005**, *16*, 2460–2467.
[9] J. Sanjurjo Sánchez, C. A. S Alves, J. R. Vidal Romanı, D. Fernández Mosquera, *Water Air Soil Pollut.* **2009**, *204*, 53–68.
[10] D. Avigo Jr., A. F. L. Godoi, P. R. Janissek, Y. Makarovska, A. Krata, S. Potgieter-Vermaak, B. Alfoldy, R. Van Grieken, R. H. M. Godoi, *Anal. Bioanal. Chem.* **2008**, *391*, 1459–1468.
[11] M. Stranger, S. S. Potgieter-Vermaak, R. Van Grieken, *Indoor Air* **2008**, *18*, 454–463.
[12] B. Horemans, A. Worobiec, A. Buczynska, K. Van Meel, R. Van Grieken, *J. Environ. Monit.* **2008**, *10*, 867–876.
[13] B. Horemans, A. Krata, A. J. Buczynska, A. C. Dirtu, K. Van Meel, R. Van Grieken, L. Bencs, *J. Environ. Monit.* **2009**, *11*, 670–677.
[14] B. Horemans, R. Van Grieken, *Atmos. Environ.* **2010**, *44*, 1497–1505.
[15] M. Strak, M. Steenhof, K. J. Krystal, I. Gosens, I. S. Mudway, F. R. Cassee, E. Lebret, B. Brunekreef, F. J. Kelly, R. M. Harrison, G. Hoek, N. A. H. Janssen, *Atmos. Environ.* **2011**, *45*, 4442–4453.
[16] B. V. Bhaskar, R. V. Rajasekhar, V. Jeba, P. Muthusubramanian, A. P. Kesarkar, *Environ. Monitor. Assessm.* **2010**, *164*, 323–336.
[17] S. S. Potgieter-Vermaak, J. H. Potgieter, R. Van Grieken, *Spectros. Europe* **2010**, *22*, 12–16.
[18] S. Nava, F. Becherini, A. Bernardi, A. Bonazza, M. Chiari, I. García-Orellana, F. Lucarelli, N. Ludwig, A. Migliori, C. Sabbioni, R. Udisti, G. Valli, R. Vecchiet, *Sci. Total Environ.* **2010**, *408*, 1403–1413.
[19] S. Potgieter-Vermaak, A. Worobiec, L. Darchuk, R. Van Grieken, Fundamentals and Applications in Aerosol Spectroscopy, (Eds: R. Signorell, J. P. Reid), Taylor and Francis, London, 2011. ISBN: 9781420085617, **2010**; p. 193-208.
[20] J. Osán, J. de Hoog, A. Worobiec, C.-U. Ro, K.-Y. Oh, I. Szalóki, R. Van Grieken, *Anal. Chim. Acta* **2001**, *446*, 211–222.
[21] B. Vekemans, K. Janssens, L. Vincze, F. Adams, P. Van Espen, *X-Ray Spectrom.* **1994**, *23*, 278–285.
[22] P. Van Espen, K. Janssens, J. Nobels, *Chemometr. Intell. Lab.* **1986**, *1*, 109–114.
[23] C.-U. Ro, J. Osan, R. Van Grieken, *Anal. Chem.* **1999**, *71*, 1521–1528.
[24] J. Osan, I. Szaloki, C.-U. Ro, R. E. Van Grieken, *Mikrochim. Acta* **2000**, *132*, 349–35523.
[25] S. S. Potgieter-Vermaak, R. Van Grieken, *Appl. Spectros.* **2006**, *60*, 39–47.
[26] Z. Shi, L. Shao, T. P. Jones, S. Lu, *J. Geophys. Res.* **2005**, *110*, D01303.

[27] B. Horemans, C. Cardell, L. Bencs, V. Kontozova-Deutsch, R. Van Grieken, *Microchem. J.* **2011**, *99*, 429–438.
[28] N. Pérez, J. Pey, X. Querol, A. Alastuey, J. M. López, M. Viana, *Atmos. Environ.* **2008**, *42*, 1677–1691.
[29] C.-U. Ro, K.-Y. Oh, H. Kim, H. Kim, H. Kim, Y. P. Kim, C. B. Lee, K.-H. Kim, C. H. Kang, J. Osán, J. de Hoog, A. Worobiec, R. Van Grieken, *Environ. Sci. Technol.* **2001**, *35*, 4487–4494.
[30] I. N. Tang, K. H. Fung, *J. Aerosol. Sci.* **1989**, *20*, 609–617.
[31] Ph. Columban, S. Cherifi, G. Despert, *J. Raman Spectrosc.* **2008**, *39*, 881–886.
[32] J. L. Díaz-Hernández, J. Párraga, *Geochim. Cosmochim. Ac.* **2008**, *72*, 3883–3906.
[33] Y. Tobo, D. Zhang, A. Matsuki, Y. Iwasaka, *Proc. Natl. Acad. Sci. U.S.A.* **2010**, *107*, 17905–17910.
[34] D. Hu, J. Chen, X. Ye, L. Li, X. Yang, *Atmos. Environ.* **2011**, *45*, 2349–2355.
[35] C. Cardell-Fernández, C. Navarette-Aguilera, *Studies in Conservation* **2006**, *51*, 161–176.
[36] C. Cardell, L. Rodriguez-Simon, I. Guerra, A. Sanchez-Navas, *Archaeometry* **2009**, *51*, 637–657.
[37] E. Kotulanova, P. Bezdicka, D. Hradil, J. Hradilova, S. Svarcove, T. Grygar, *J. Cultural Heritage* **2009**, *10*, 367–378.
[38] C. M. Grossi, P. Brimblecombe, B. Menéndez, D. Benavente, I. Harris, M. Déqué, *STOTEN, Sci. Total Environ.* **2011**, *409*, 2577–2585.